Vol. 14(4), pp. 69-80, October-December 2020
DOI: 10.5897/AJPAC2019.0827
Article Number: 10B09D764989
ISSN: 1996 - 0840

http://www.academicjournals.org/AJPAC

ACADEMIC JOURNALS
expand your knowledge

African Journal of Pure and Applied Chemistry

Full Length Research Paper

Catalytic activity of using tungsten oxide with hydrogen peroxide for methyl orange degradation

Séverin N'goran EROI[1], Aimé Serge ELLO[1]*, Donourou DIABATE[1], Diby Benjamin OSSONON[2] and Jocelin Martial YAO[3]

[1]Laboratoire de Chimie Physique, 22 bp 582 Abidjan 22, Université Felix Houphouët-Boigny, Côte d'ivoire.
[2]Institut National de Recherche Scientifique-Énergie, Matériaux et Télécommunications (INRS-EMT) 1650, Boulevard Lionel-Boulet Varennes (Québec) J3X 1S2 Canada.
[3]Université de Haute-Alsace, CNRS, Institut de Science des Matériaux de Mulhouse (IS2M), UMR 7361, F-68093 Mulhouse, France.

Received 19 December 2019; Accepted 1 June 2020

In this work, a tungsten oxide nanoparticle was developed with a simple method, using tungsten powder. The orthorhombic, hexagonal and monoclinic crystalline structures obtained were characterized by X-ray diffraction, scanning electron microscopy, as well as Fourier transform infrared spectroscopy and X-ray photoelectron spectroscopy. The coupling of these tungsten oxide nano particles with hydrogen peroxide is carried out on methyl orange removal from wastewater. The use of Hydrated orthorhombic particles showed the highest removal rate up to 89.7% comparatively to hexagonal and monoclinic crystalline structures respectively. The reusability of these particles showed a good stability with monoclinic crystalline structure after four cycles.

Key words: Dyes, Tungsten Oxide, Catalysis, H_2O_2.we

INTRODUCTION

Azo dyes are present in wastewaters from the textile, paper, plastics, leather, food, cosmetics and some other industries. Unfortunately, they constitute one of the major sources of environmental degradation of water (Pavithra et al., 2019). Azo dyes are not only dangerous to aquatic life, but in many cases carcinogenic to humans and animals (Fatima et al., 2017). Researchers are thinking about creating an effective technique for the removal of pestilent dyes from wastewaters. Several methods like adsorption (Ayati et al., 2016), hydrogenation (Fu et al., 2019), photocatalysis (Yang et al., 2018, 2019; Chen et al., 2019; Zeng et al., 2019; Feng et al., 2020), degradation by biological (Rajasulochana and Preethy, 2016) and chemical oxidation (Collivignarelli et al., 2019; Katheresan et al., 2018) have been applied for industrial wastewaters remediation before their disposal to the environment. The use of hydrogen peroxide as an oxidizing agent was also proposed for a long time but proved to be ineffective when the load of dye is high (Wang et al., 2016). So, research groups have been focused on advanced oxidation processes, some environmentally friendly methods allow treatment of dyes in wastewater. These technologies have already shown their potential in treating toxic and biologically recalcitrant organic pollutants. The advanced oxidation processes include O_3 (Biard et al., 2018), UV (Seo et al., 2019),

*Corresponding author. E-mail: aime.ello@univ-fhb.edu.ci.

UV/H_2O_2, (Li et al., 2020), O_3/UV (Wardenier et al., 2019), and Fenton (Bello et al., 2019; Zhu et al., 2019; Xiao et al., 2020). Among all advanced oxidation processes, Fenton reaction using soluble iron salts in $Fe2^+$ or Fe^{3+} form and H_2O_2 can produce powerfully oxidizing radical species such $HO^•$ ($Fe^{2+} + H_2O_2 \rightarrow Fe3^+ + HO^• + OH^-$ (1) $Fe^{3+} + H_2O_2 \rightarrow Fe^{2+} + HO_2^• + H^+$ (2)) for decomposition of dyes. However, the implementation of homogeneous Fenton oxidation based on ferrous or ferric salts has several limitations, including the conversion of $Fe(OH)_3$ into sludge at a pH above 4 (Zhu et al., 2019) which requires an additional treatment (Cetinkaya et al., 2018) and a cost for their elimination. To improve the oxidation efficiency heterogeneous Fenton-like reaction has been developed. Heterogeneous Fenton-like processes can be established by replacing Fe^{2+} in the Fenton reagent with a solid catalyst including metal oxide. According to literature (Thornburg et al., 2016; Ziolek et al., 2015; Ziolek and Sobezak, 2017) reactive oxygen species can be generated in situ on the surface of selected metal oxides (such as Nb_2O_5, V_2O_5, TiO_2, Fe_2O_3) by the treatment with hydrogen peroxide, and then successfully used as heterogeneous catalysts for degradation of organic pollutants (Bello et al., 2019; Wiedmer et al., 2016; Zhu et al., 2019). The advantages of using metal oxide as solid catalyst in heterogeneous Fenton-like process comparatively to homogeneous Fenton process are: (a) The reactions shows performance in a wide range of pH (Zhu et al., 2019) (b) metal oxides can be recovered easily; (c) metal oxides decompose hydrogen peroxide H_2O_2 to hydroxyl radical $HO^•$ like in classical Fenton reaction, and prevent precipitating of iron hydroxide (sludge) which reduce the efficiency of global oxidation process (Zhu et al., 2019). Among the heterogeneous Fenton-like processes, Photo-Fenton has been developed as a promising method using catalysts such Fe_2O_3 (Domacena et al., 2020), Fe_3O_4, (Arshad et al., 2017) FeOOH (Liu et al., 2017), Fe_2O_3/Al_2O_3 (Di Lucia et al., 2018) to overcome the classic homogeneous Fenton drawbacks mentioned above. However, UV and Visible light-based photo Fenton oxidation also has practical limitations. At neutral pH, a photo Fenton process showed low efficiency and needed the addition of iron complexing agents (Ahile et al., 2019). Consequently, significant efforts to develop various new heterogeneous Fenton catalysts have been made including; CuO (Deka et al., 2016), CeO_3 (Wei et al., 2019) and Mn_3O_4 (Osgouei et al., 2020). The aim of this work is to propose a new alternative metal oxide such as tungsten oxide coupled with H_2O_2 for the treatment of methyl orange. WO_3 can be a remarkable candidate as solid Fenton catalyst because in nano size, transition metal oxides has a great interest for oxidation due to is large surface area, which exhibits many advantages in the chemical catalysis field, such as a low diffusion resistance, easy accessibility to reactants, and large number of active sites (Gadipelly and Mannepalli, 2019). The use of WOx/H_2O_2 has not been reported in the literature as heterogeneous Fenton-like process. Thus, to evaluate the outstanding efficiency using the WO_3 catalyst, a comparative study with other metal oxides for removal methyl orange from aqueous solution was presented.

MATERIALS AND METHODS

Experimental

Tungsten oxide NPs were prepared by a simple dispersion of metallic tungsten powder (1.0 g) (APS 1-5 µm, purity 99,9%, Alfa Aesar Co.) in deionized water (10 ml), glacial acetic acid (1 ml , ACS reagent, purity ≥99.7%) followed by addition of H_2O_2 (10 ml, aqueous solution; 30%, Fisher Scientific Co.) dropwise. The mixture was kept at 0°C in an ice bath. The oxidative dissolution process was very exothermic; therefore it was realized carefully under a well-ventilated fume hood. The solution was put in the glass reactor equipped with a condenser and heated at 85 °C for 3h. A precipitate is formed and centrifuged at 8000 rpm. Hydrated tungsten oxide WO_3-H_2O material was obtained without any surfactant by washing the precipitate with water and ethano,l then dried at 60°C overnight (16 h). Hydrated tungsten oxide WO_3-H_2O material followed two treatments: it was annealed at 200 and 600°C for 4 h and obtained h-WO_3 and WO_3 respectively.

Characterization

Powder X-ray diffraction (XRD) patterns of the samples were obtained on a Bruker D8 Advance X-ray diffractometer equipped with a Cu Kα radiation source (λ = 1.5418 Å). Fourier transform infrared (FTIR) absorption spectra were measured with an FTS 45 infrared spectrophotometer using KBr pellet technique. Scanning electron microscopy (SEM) images were taken on a JEOL 6360 instrument at an accelerating voltage of 3 kV. X-ray photoelectron spectroscopy (XPS) measurements were performed on a VG Escalab 220i-XL using a polychromatic Al source (hv = 1486.6 eV) operating at 15 kV and 20 mA. The signal was filtered with a hemispherical analyser (pass energy = 20 eV) and the detection was performed with a multi-channel detector. The base pressure inside the spectrometer during analysis was 3×10^{-10} Torr.

Catalytic tests

Catalytic tests were carried out in a reactor capacity of 250 ml attached with a condenser. 100 ml of aqueous solution of methyl orange was introduced and 50 mg of various tungsten oxides obtained following 2.5 ml of H_2O_2. The reactor was put in the oil bath previously heated and maintained at 65°C. During the reaction, the mixture was continuously stirred using magnetic stirrer (agitation rate ~ 400 rpm) for 3 h. The residual concentration of dye in the aqueous solution was determined each 20 min via UV-vis spectrophotometer at 464 nm. At the end of the reaction time, the tungsten metal oxide particles were separated from aqueous solution by using centrifuge at 8000 rpm during 10 min. Tungsten metal oxide particles were recovered then washed with ethanol and water several times and dried at 60°C overnight for reusability.

RESULTS

XRD analysis is considered a promising technique,

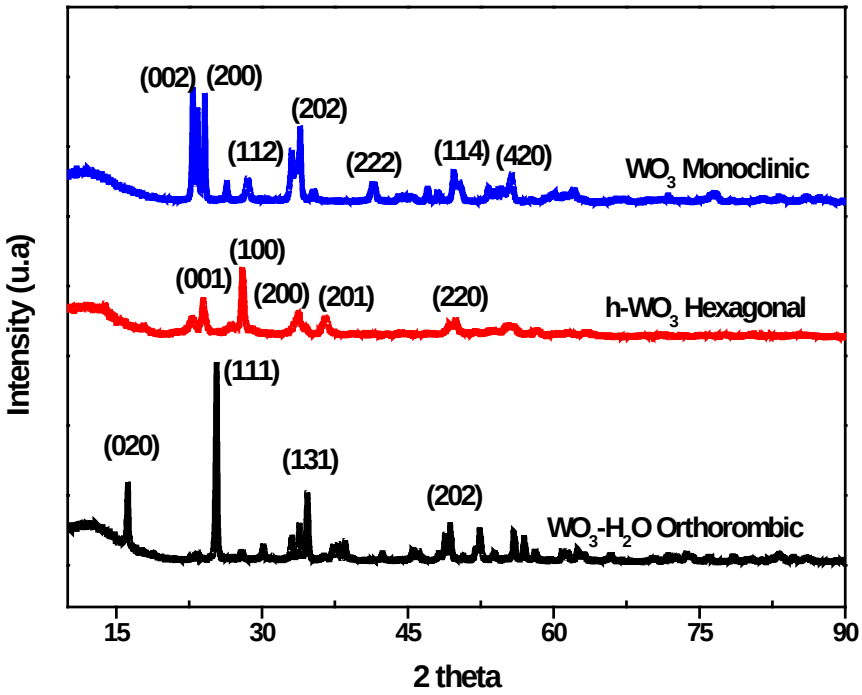

Figure 1. XRD patterns of WO_3-H_2O orthorombic, h-WO_3, hexagonal at 200°C and WO_3 monoclinic at 600°C.

investigating the crystalline structure and size of the synthesized nanoparticles. Figure 1 displays the XRD pattern of the synthesized tungsten oxide nanoparticles before and after calcination. The precipitate obtained showed various diffraction peaks at 2θ = 16, 53; 25, 63; 35, 03 and 49, 64 which are assigned to (020), (111), (131) and (202) reflections according to the JCDPS card N° (84-0886). This crystalline structure is identical to hydrated tungsten oxide WO_3-H_2O of orthorhombic structure. This type of structure was also observed in the case of hydrothermal and solvothermal synthesis of tungsten oxide nanoparticles for sensing volatile organic compound (Perfecto et al., 2016) and photocatalytic activity (Liu et al., 2019), respectively. The calcination of WO_3-H_2O at 200 and 600°C respectively showed different XRD patterns. At 200°C diffraction peaks were in agreement with the hexagonal phase of WO_3 (JCDPD card N° 75-2187). The h-WO_3 hexagonal phase was also observed after calcination treatment (Perfecto et al., 2016). The peaks corresponding to (100), (001), (200) and (2011) crystal planes were also identified. Increasing the calcination temperature up to 600°C showed the peaks assigned to WO_3 monoclinic structure (JCDPD card $N_0$71-2141). These peaks appeared at 2θ values of = 23.12; 23.58; 24.38; 26.59; 28.93; 33.26; 34.17; 41.9 having miller indices (002), (020), (200), (123) (112), (022), (220), (222) respectively (JCDPD card $N_0$71-2141). This monoclinic crystalline structure had been shown at this temperature previously (Kang et al., 2020) and increasing the calcination temperature up to 450°C produced a stable monoclinic phase (Salkar et al., 2018).

In order to investigate the surface morphology of these tungsten oxide particles, scanning electron microscopy was carried out for the various samples. Figure 2 shows morphology of the tungsten oxides particles.

Figure 2A shows the nanoplates obtained before calcination. The shape evolved with the temperature of calcination, giving nanorod-like structure (Figure 2B) at 200°C and pallets with large thickness at 600°C (Figure 2C). The particles are not uniform in micro or nano size but regular without addition of surfactant. The X-ray photoelectron spectroscopy (XPS) is a useful tool to investigate the composition and oxidation states of elements presented over the surface of the tungsten oxide particles. Figure 3A shows a wide survey scan of the samples, clearly indicating the presence of W and O elements. The deconvolution of W4f spectrum in Figure 3B clearly shows two peaks at 35.6 and 37. 7 eV which were assigned to W $4f_{7/2}$ and W$4f_{5/2}$ respectively for WO_3-H_2O. The binding energy at 35.7 and 37.8 eV were assigned to W$4f_{7/2}$ and W $4f_{5/2}$ for h-WO_3, while the peaks located at 35.4 and 37.5 eV were attributed to W $4f_{7/2}$ and W $4f_{5/2}$ of monoclinic WO_3.

XPS analysis is one of the fundamental tool and the Figure 3B depicted, two spin-orbit doublets corresponding to the different valence states of W. This spin-orbit splitting of W4f is 2.1 eV for all tungsten oxides, which agrees with previously published literature for W^{6+}

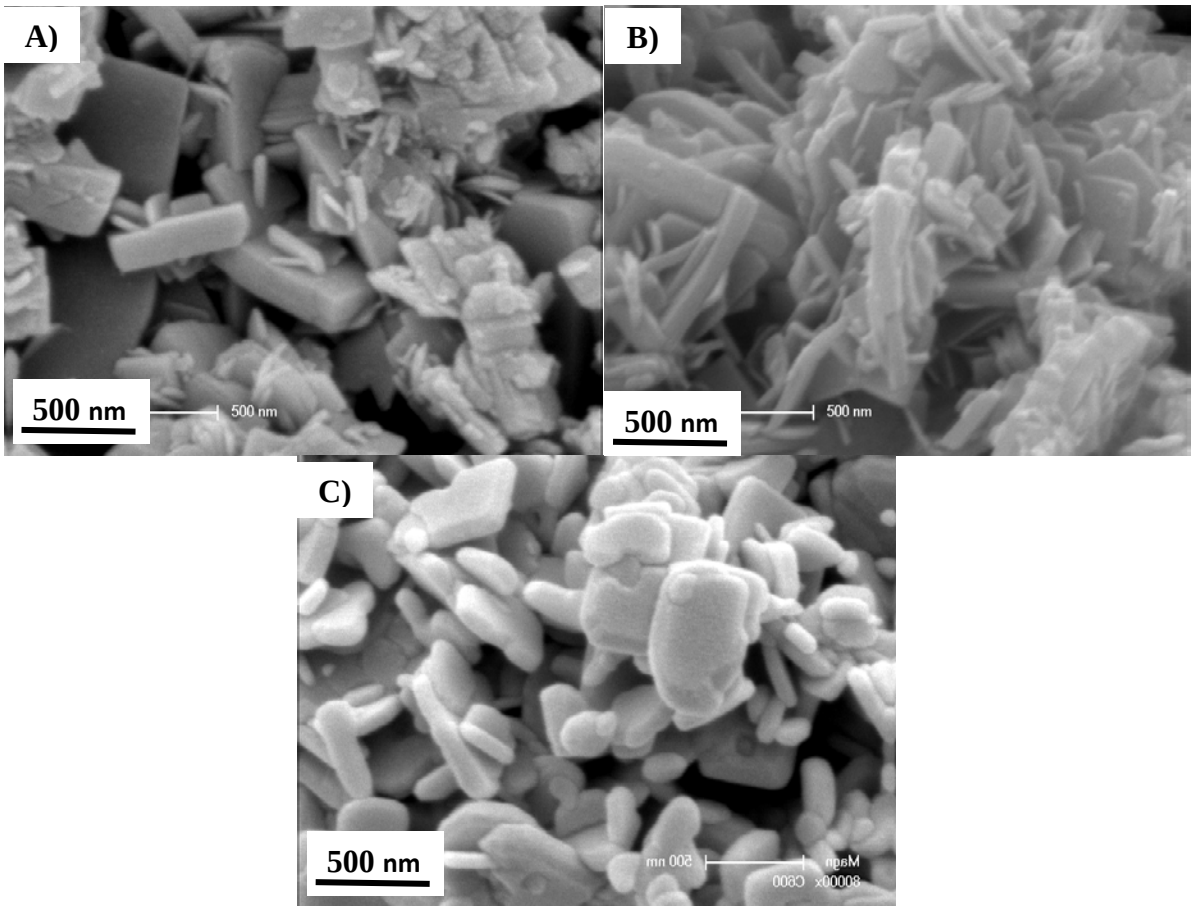

Figure 2. SEM images of synthesized WO_3 (A) $WO_3.H_2O$ orthorhombic, (B) h-WO_3 hexagonal, (C) WO_3 monoclinic structure.

ions or +6 oxidation state (Kolhe et al., 2020). Figure 3C shows O1s spectra. The deconvolution of these peaks showed various weak peaks at different binding energy only for h-WO_3 and WO_3-H_2O. The monoclinic tungsten oxide structure showed a peak at 530 eV and both h-WO_3 and WO_3-H_2O samples at 530,2 eV which are attributed to the lattice oxygen bonded with W (Parthibavarman et al., 2018). WO_3-H_2O showed a high peak of adsorbed H_2O at 532.5 eV which confirms XDR results. The peak of adsorbed H_2O shifted to a weak at 532.4 eV due to a very small amount of water containing h-WO_3. The peak at 531.4 eV is due to OH groups. XPS study strongly supported the formation of WO_3 and confirmed XRD patterns observed for tungsten oxide structures. The same results were observed by several authors during the synthesis of tungsten oxide (Thornburg et al., 2016; Kolhe et al., 2020; Parthibavarman et al., 2018). The small characteristic peak of the carbon element is observed at 284 eV in Figure 3A and is attributed to the carbon dioxide of the air or to the impurities of the reagents or to the washing solvent. These same results were demonstrated by Geng et al. (2017). Figure 4 shows the FT-IR spectra of the various tungsten oxide synthesized.

Identification of molecular structures reveals normal vibration modes by stretching (v), plane bending (δ). The vibration bands are mainly the fundamental vibrations of the W=O, W-O and W-O-W chromophores and the stretching of O-W-O bonds (Ziolek et al., 2015). Below 1000 cm^{-1}, the FT-IR spectra showed significantly various vibration peaks at 942 and 671 cm^{-1} assigned as the stretching of W=O and O-W bonds in the hydrated tungsten oxide WO_3-H_2O crystalline structure. These stretching bonds exist also in both hexagonal and monoclinic structure. The increase of the calcination temperature up to 600°C created a characteristic peak of O-W-O stretching vibrations in the WO_3 monoclinic crystal lattice.

The absence of carbonyl peak around 1730 cm^{-1} indicated that no carbon contained all the samples, which confirmed the impurities shown in XPS spectra (Figure 3A). For hydrated tungsten oxide, the symmetric stretching vibrations related to WO_3 were observed and the intercalated water molecules (W-OH ... H_2O) are

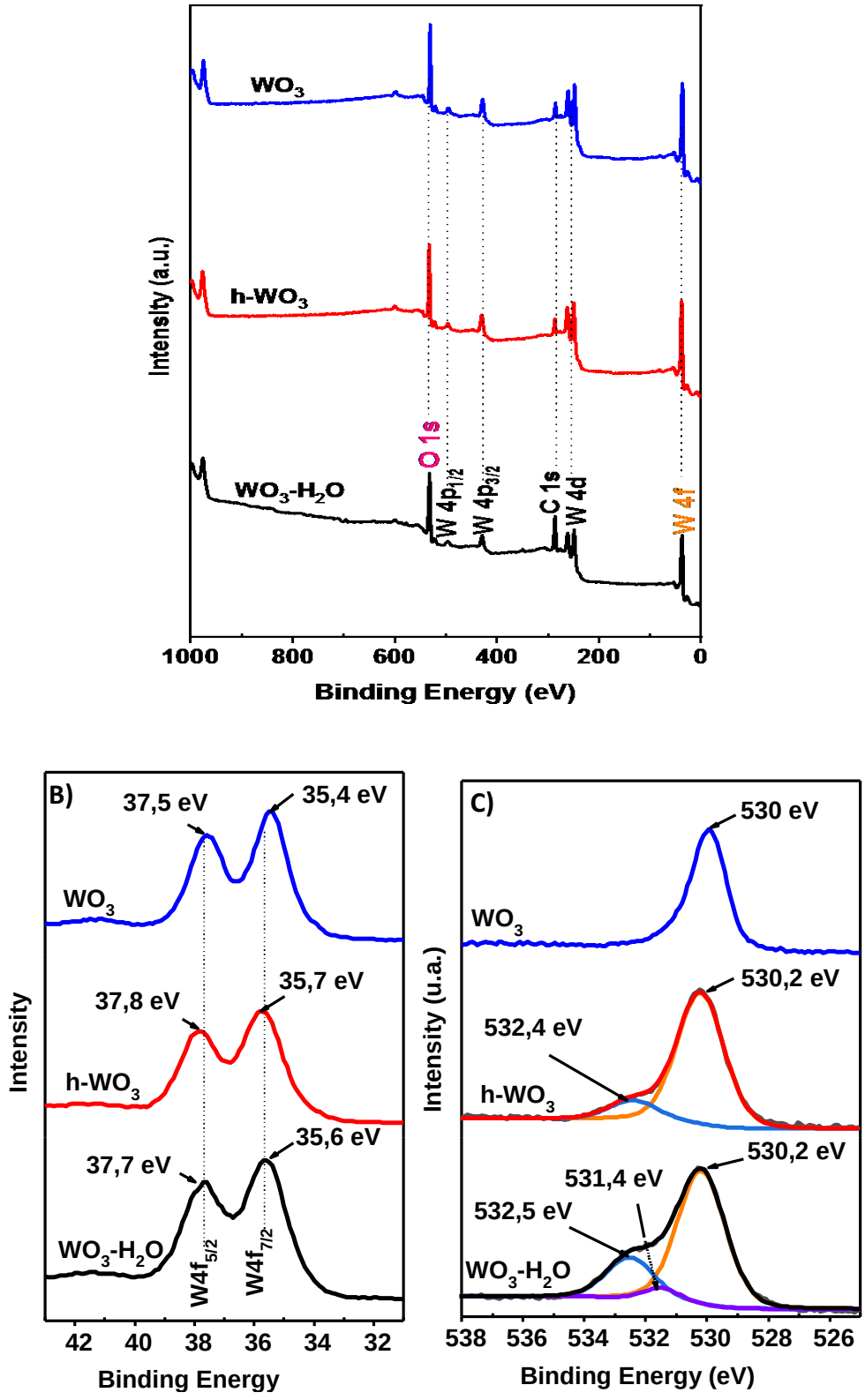

Figure 3. XPS spectra of (A) full scan survey of synthesized WO_3, (B) W4f, (C) 1Os.

characterized by a significant peak at 3397 cm^{-1}. The bending vibration is observable at approximately δ =

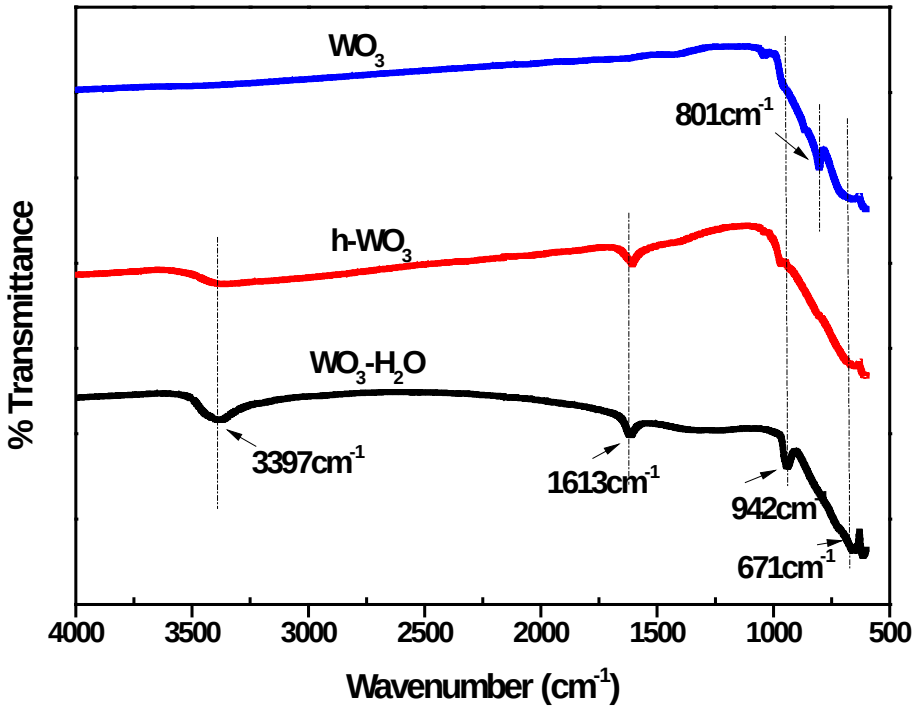

Figure 4. FT-IR spectra of WO_3-H_2O. h-WO_3, and WO_3

1613 cm^{-1} which corresponds to the W-OH plane for the WO_3-H_2O. These vibrations generate the presence of H_2O, which confirms the orthorhombic WO_3-H_2O structure observed in XRD and H_2O absorbed in XPS. Indeed, WO_3-H_2O was obtained at 85°C without calcination, that did not allow removal of water molecules; thus creating their inter reaction with tungsten oxide structure. The peak at 3397 cm^{-1} is weak and not significant for the h-WO_3 comparatively to WO_3-H_2O structure. The bending vibration is observable at approximately δ = 1613 cm^{-1}. The h-WO_3 shows that water molecules are removed but there is a small amount intercalated water molecules containing on the plane. The water intercalated was shown by XPS (Figure 3C). Increasing the calcination temperature up to 600°C removed water and led to obtain non-hydrated crystal structure WO_3 because there are no vibration peaks in the range of 3000-3700 cm^{-1} corresponding to the presence of water. These results confirmed structures proposed by XRD and XPS.

Catalytic activity

The catalytic activities of tungsten oxides nanoparticles synthesized were carried out on the capacity of methyl orange remove from an aqueous solution. Efficiency of the removal process was monitored by UV-visible spectroscopy. Figure 5 shows the methyl orange removal rate, using tungsten oxide nanoparticles with hydrogen peroxide.

Hydrated tungsten oxide WO_3-H_2O alone eliminated around 3% of methyl orange after 3 h. The amount of methyl orange removed, increased up to 10% when H_2O_2 was also used only, slightly high comparatively to hydrated tungsten oxide WO_3-H_2O. According to the literature, it is possible to oxidize many organic compounds with hydrogen peroxide (Zhang et al., 2019). Coupling H_2O_2 and the tungsten oxides nano particles increased the removal efficiency of methyl orange. The values reached 20, 30 and 47% for the coupling of hydrogen peroxide with WO_3, h-WO_3 and WO_3-H_2O catalysts respectively. The use of hydrogen peroxide with tungsten oxide nanoparticles had a benefit effect for methyl orange removal. Many authors had shown that the catalytic activity of metal oxides in dye degradation is enhanced when metal oxides are combined with hydrogen peroxide in acid pH medium (Ziolek and Sobezak, 2017; Osgouei et al., 2020; Deka et al., 2016). The reaction of these tungsten oxide nanoparticles with H_2O_2 led to generation of strongly reactive oxidative species such as $O_2^{\bullet-}$ and O_2^{2-} , $HO^{\bullet}$ (Ziolek et al., 2015). All the catalytic tests were carried out at pH = 6.9 that is very difficult in classical Fenton process. The coupling of WO_3-H_2O with hydrogen peroxide displayed a high performance comparatively to h-WO_3 and WO_3 respectively. Therefore, WO_3-H_2O led to formation of more reactive oxygen species than h-WO_3 and WO_3. The presence of water in crystal lattice increased the ability of WO_3-H_2O to generate more oxidative species. Thus, the high production of hydroxyl radicals in the presence of

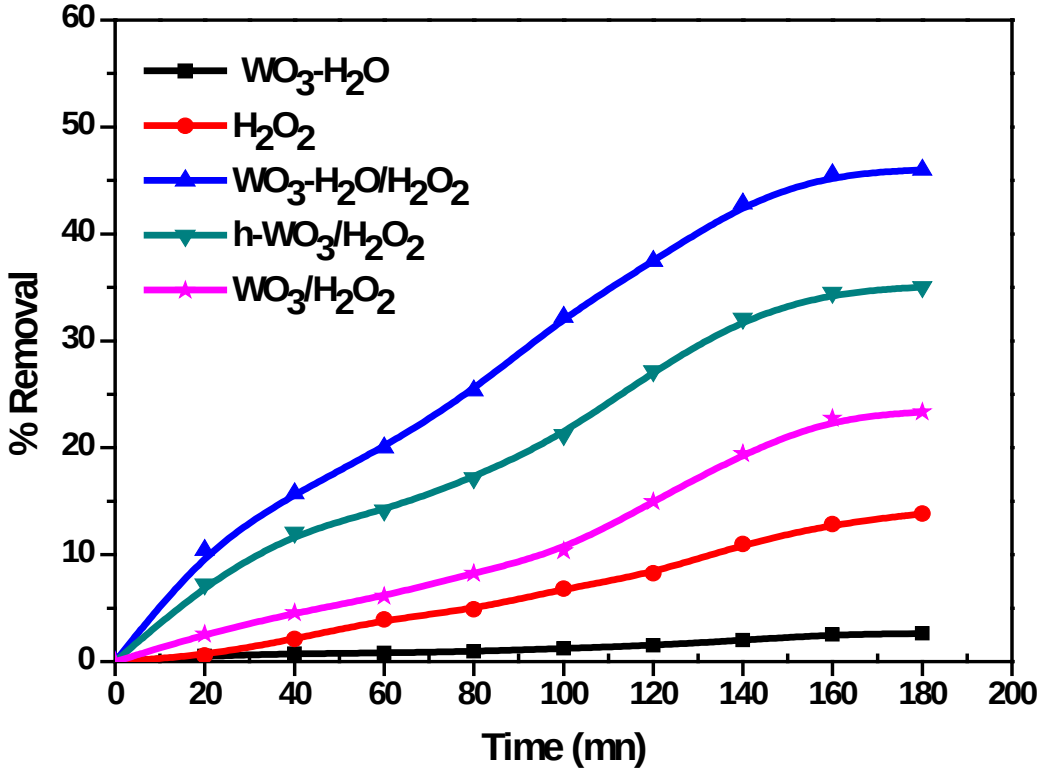

Figure 5. Removal of methyl orange by using WO_3-H_2O, h-WO_3 and WO_3 with or not H_2O_2 at pH=6.9.

water by the hydrated orthorhombic structure of tungsten oxide caused significant degradation of methyl orange comparatively to the hexagonal and monoclinic structures respectively. The reaction of H_2O_2 with the metal oxides is very complex, but the mechanism for production of hydroxyl radicals is known and consists of two steps: adsorption of H_2O_2 on metal oxide followed by its decomposition or cleavage to form hydroxyl radicals (Lousada et al., 2015). These two steps are also governed by the state of metal oxide surface and the kinetics of decomposition respectively (Lousada et al., 2015).

The hydrated structures of tungsten oxide promoted the kinetics of hydrogen peroxide cleavage for the production of hydroxyl radicals. It is known that the kinetics of decomposition is strongly influenced by the pH of the reaction medium (Lousada et al., 2015; Wolski et al., 2019). To increase the performance of hydrated tungsten oxide, the catalytic reaction tests were done at a pH range as shown in Figure 6. The methyl orange removal rate increased when the pH medium decreased and maximum of methyl orange removal reached up 51% when the pH medium is 4. The results confirmed that shown in precious literature (Lousada et al., 2015; Wolski et al., 2019). The mass effect was also realized. Figure 7 displayed that the high rate of methyl orange removal was observed when the mass is 300 mg for WO_3-H_2O and WO_3. At this mass value, the methyl orange removal reached up to 89.7 and 74.4% for WO_3-H_2O and WO_3 respectively. Thus, increasing the mass of tungsten oxide led to considerable removal of methyl orange from water. The UV-vis absorption spectra of methyl orange were recorded and shown in Figure 8. The spectrum of initial methyl orange shows two peaks located at 464 nm from the azo bond and at 298 nm attributed to benzene nucleus in the methyl orange molecule before treatment. After the end of reaction time of degradation, the decrease in these peaks was observed when H_2O_2 is used, indicating that the azo bond was destroyed. The treatment of methyl orange with the coupling WO_3-H_2O/H_2O_2 showed that the absorption peak from the azo bond decreased considerably, while the absorption at 298 nm from the benzene nucleus increase drastically and shifted to 288 nm, indicating that degradation intermediates containing the benzene ring were generated. These results are consistent with the work reported in previous literature (Chen et al., 2015; Omri et al., 2020).

The efficiently of monoclinic WO_3 is also increased. It was essential to compare the efficiency of the heterogeneous Fenton-like system using tungsten oxide for the removal of methyl orange with another heterogeneous Fenton-like system using other metal oxides. The Table 1 showed the performance of the Fenton-like process obtained with different metal oxides for the removal of methyl orange only. As showed in

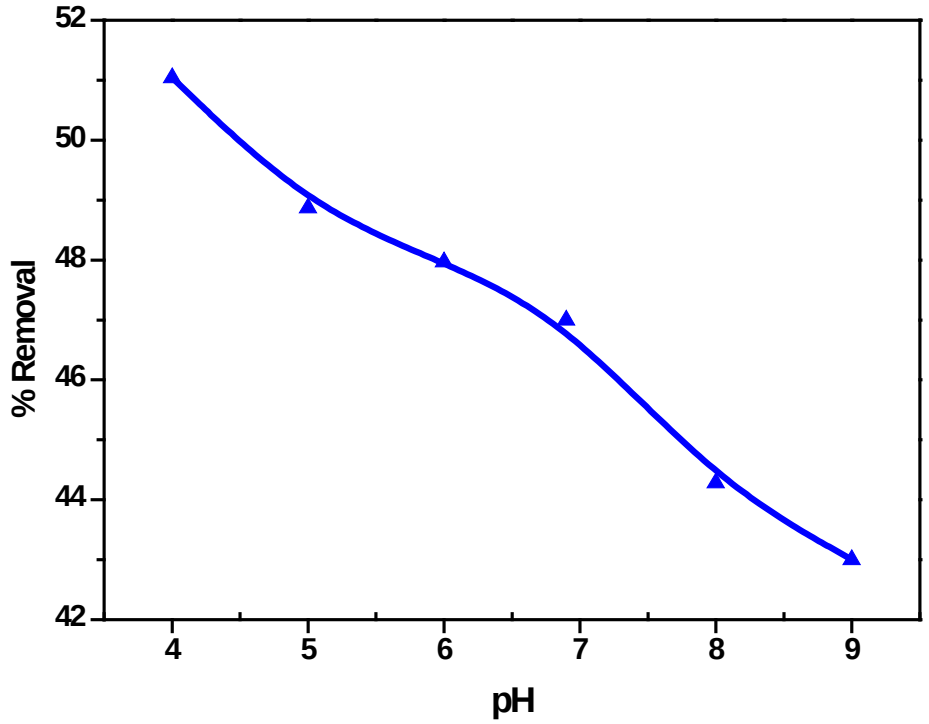

Figure 6. Influence of pH for methyl orange removal using WO_3-H_2O/H_2O_2.

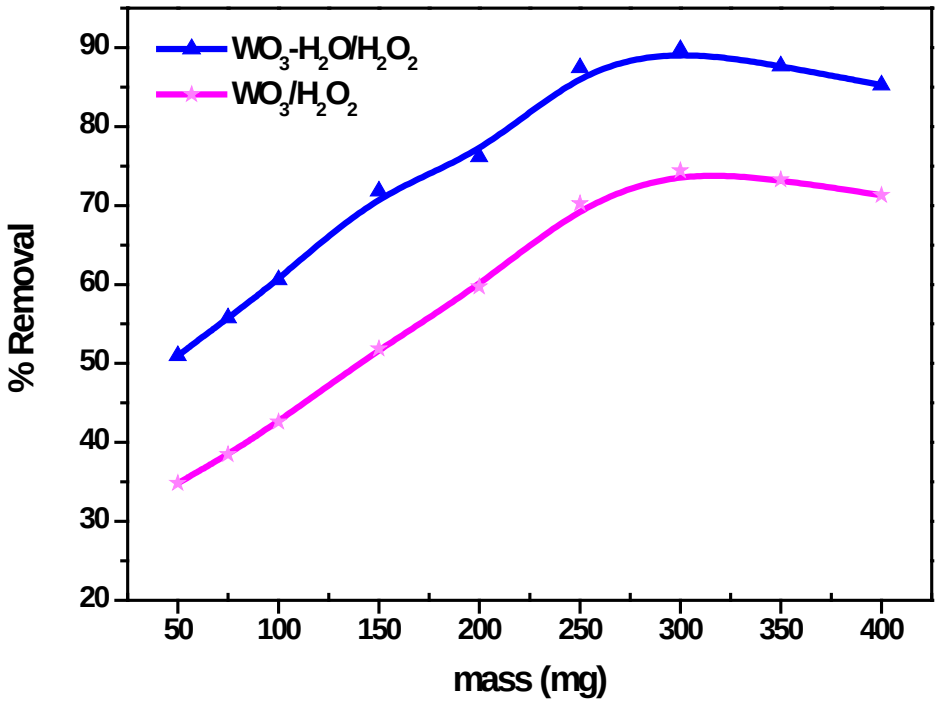

Figure 7. The mass effect of WO_3-H_2O and WO_3 on dye removal at pH=4.

Table 1, the results of the study are higher than iron oxide, titanium oxide nanoparticles capacities. The supported metal oxides showed higher performance. All of these others metal oxide used photo Fenton as a Fenton-like process which used UV or Visible light to increase radical hydroxyl amount. The Fenton-like

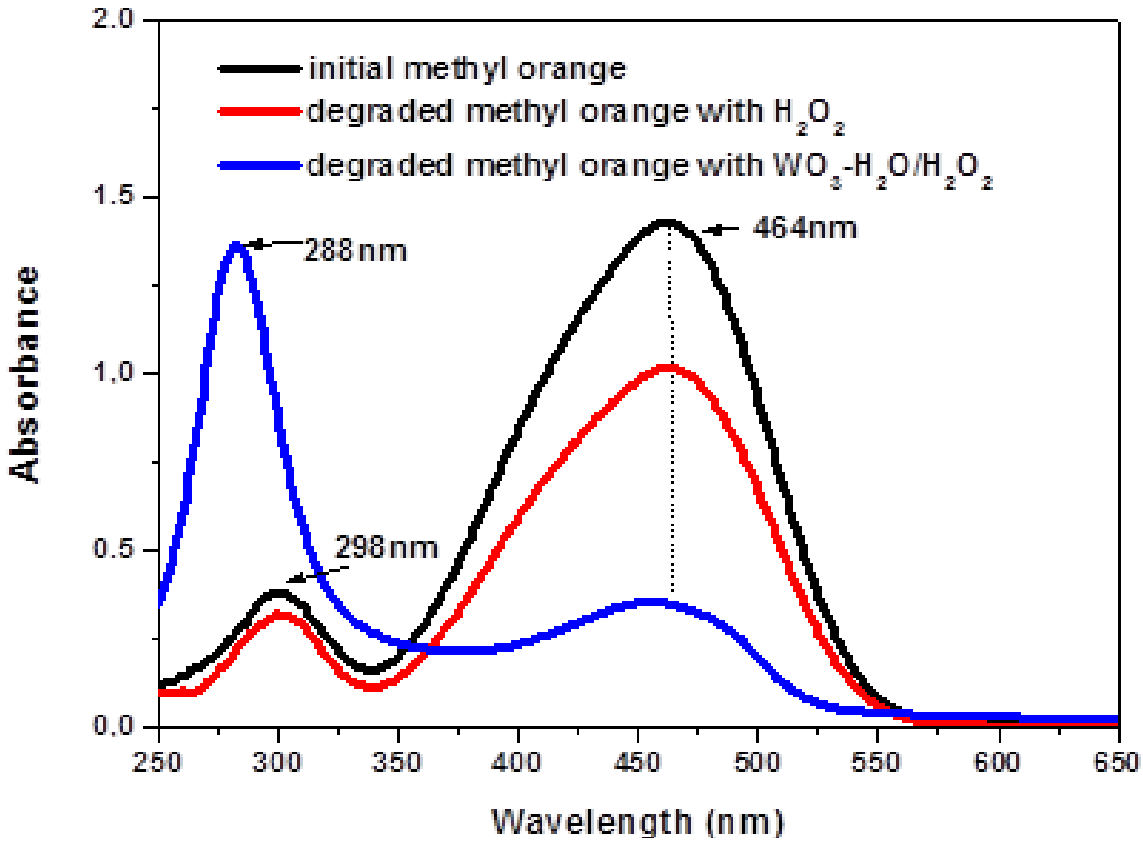

Figure 8. UV-vis spectra of the original and degraded methyl orange at pH=4.

Table 1. The performance of Fenton-like process catalysts used for methyl orange removal.

Heterogeneous catalysts	Removal (%)	References
Graphene /Fe_3O_4	99.24	Arshad et al. (2017)
Fe_3O_4	43	Arshad et al. (2017)
Nano TiO2	60	Chen et al. (2018)
Fe_2O_3	76.5	Domacena et al. (2020)
Fe_2O_3/TiO_2	98	Hassan et al. (2016)
Cu_2O	80-95	Zhang et al. (2018)
WO_3-H_2O	89.7	Our study
WO_3	74.4	Our study

process using tungsten metal oxide nanoparticle requires no UV input and showed high performance at pH= 4 in comparison to these other metal oxides, which need more strong acid pH medium.

Reusability of the tungsten oxide nanoparticles was investigated. Unfortunately, it was difficult to do more than 2 cycles of methyl orange removal with WO_3-H_2O because of the loss of hydrated tungsten oxide particles as well as the leaching. As shown in SEM analysis, WO_3-H_2O showed the small size particles comparatively to monoclinic WO_3. It was then, not so easy to recover these particles. However, monoclinic WO_3 particles were recovered easily and reused in 4 consecutive runs. As shown in Figure 9, the removal efficiencies of WO_3 found are 74.4; 73. 2; 71.3 and 69.6% in first cycle, second, third and fourth cycle respectively. A slight loss was observed in efficiency of monoclinic tungsten metal oxide nanoparticles. Monoclinic WO_3 showed excellent stability even after four continuous cycles of activity, whereas the removal efficiency of monoclinic WO_3 is relatively

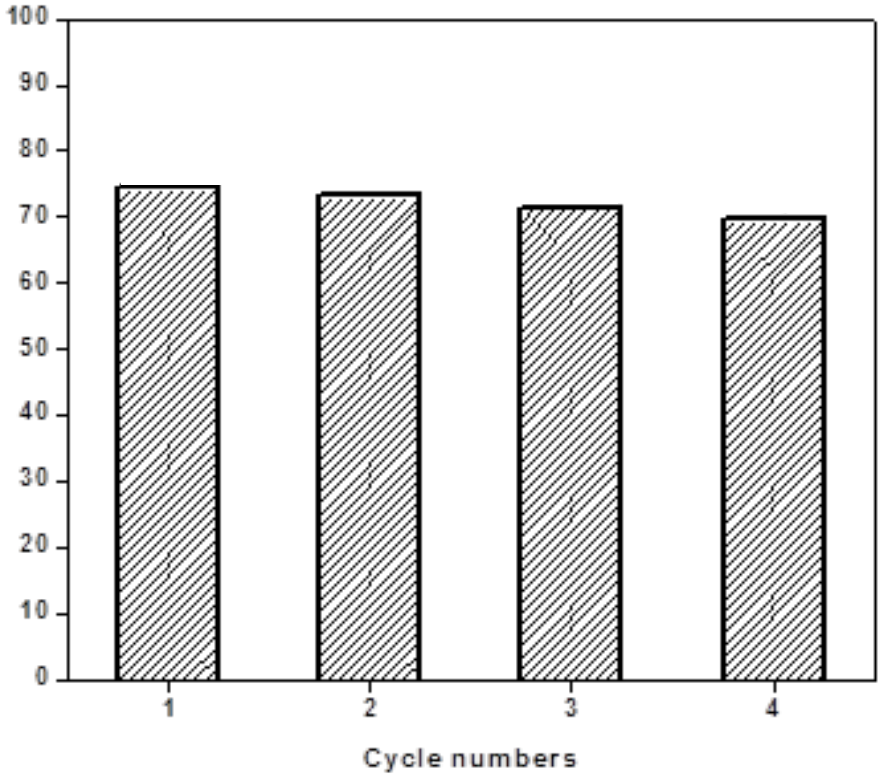

Figure 9. Recyclability and reusability tests of monoclinic WO_3.

reduced after four cycles of reusability.

Conclusion

This study demonstrated that the combination of tungsten oxide nanoparticles with hydrogen peroxide as a Fenton-like system improved the removal of methyl orange from water. This process did not need pH = 3 condition to show high performances. The tungsten oxide particles in nano size have been well identified and characterized by various technical. Coupling the tungsten oxide nanoparticles with H_2O_2 showed high methyl orange removal rate comparatively to hydrogen peroxide or tungsten oxide used alone. At pH = 4, the increase of the mass of tungsten oxides nanoparticles produced better conditions with H_2O_2 to form more reactive oxygen species attributed to orthorhombic tungsten oxide WO_3-H_2O comparatively to h-WO_3 and WO_3. The reusability of the monoclinic WO_3 was done and showed good stability. The Fenton-like process using WO_3/H_2O_2 showed higher capacity to remove methyl orange than many other metal oxides associated with hydrogen peroxide.

CONFLICT OF INTERESTS

The authors have not declared any conflict of interests.

ACKNOWLEDGMENTS

The authors appreciate the government of Côte d'Ivoire under the Research Program of Merit Student for the support. The authors also acknowledge the Institut National de Recherche Scientifique-Énergie, Matériaux et Télécommunications (INRS-EMT) of Canada and the Institut de Science des Matériaux de Mulhouse (IS2M), of France for their cooperation.

REFERENCES

Ahile UJ, Wuana RA, Itodo AU, Sha'Ato R, Dantas R. F (2019). A review on the use of chelating agents as an alternative to promote photo Fenton at neutral pH: Current trends, knowledge gap and future studies. Science of Total Environment 710:134872.

Arshad A, Iqbal JI, Ahmad (2017). Graphene/Fe_3O_4 nanocomposite: interplay between photo-Fenton type reaction, and carbon purity for the removal of methyl orange. Ceramics International 44(3):2643-2648

Ayati A, Shahrak NM, Tanhaei B, Sillanpää M (2016). Emerging adsorptive removal .of azo dye by metal-organic frameworks. Chemosphere 160:30-44.

Bello MM, Raman AA, Asghar A (2019). A review on approaches for addressing the limitations of Fenton oxidation for recalcitrant wastewater treatment. Process Safety and Environmental Protection 126:119-140.

Biard PF, Dang Thom TBJ, Couvert A (2018). Intensification of the O_3/H_2O_2 advanced oxidation process using a continuous tubular reactor filled with static mixers: proof of concept. Chemical Engineering Journal 344:574-582.

Cetinkaya SG, Morcali MH, Akarsu S, Ziba CA, Dolaz M (2018). Comparison of classic Fenton with ultrasound Fenton processes on industrial textile wastewater. Sustainable Environment Research 28:165-170.

Chen T, Jiang C, Wang C, Sun J, Wang X, Li X (2015). A TiO_2 modified abiotic-biotic process for the degradation of the azo dye methyl orange. RSC Advance 5:58704.

Chen XF, Lin SR, Kou SC (2018). Effect of composite photo-catalysts prepared with recycled clay brick sands and nano-TiO_2 on methyl orange and NOx removal. Construction and Building Materials 171:152-160.

Chen Y, Zhao C, Ma S, Xing P, Hu X, Wu Y, He Y (2019). Fabrication of Z-scheme AgBr/Bi_4O5Br_2 nanocomposite and its high efficiency in photocatalytic N_2 fixation and dyes degradation. Inorganic Chemistry Frontiers 6(11):3083-3092.

Collivignarelli MC, Abbà A, Miino MC, Damiani S (2019). Treatments for color removal from wastewater: State of the art. Journal of Environmental Management 236:727-745.

Deka P, Hazarika A, Deka RC, Bharali P (2016). Influence of CuO morphology on enhanced catalytic degradation of methylene blue and methyl orange. RSC Advances 6(97):95292-95305.

Di LC, Massa P, Grau JM, Marchetti SG, Fenoglio R, Haure P (2018). Highly dispersed Fe^{3+}-Al_2O_3 for the Fenton-like oxidation of phenol in a continuous up-flow fixed bed reactor Enhancing catalyst stability through operating conditions. Applied Catalysis B: Environmental 237:1110-1123

Domacena AMG, Aquino CLE, Balela MDL (2020). Photo-Fenton Degradation of Methyl Orange Using Hematite (α-Fe_2O_3) of Various Morphologies. Materials Today: Proceedings 22:248-254.

Fatima M, Farooq R, Lindström RW, Saeed M (2017). A review on biocatalytic decomposition of azo dyes and electrons recovery. Journal of Molecular Liquids 246:275-281.

Feng Z , Zeng L, Zhang Q, Ge S, Zhao X, Lin H, He Y (2020). In situ preparation of g-C_3N_4/$Bi_4O_5I_2$ complex and its elevated photo activity in Methyl Orange degradation under visible light. Journal of Environmental Sciences 87:149-162.

Fu Y, Qin L, Huang D, Zeng G, Lai C, Li B, He J, Yi H, Zhang M, Cheng , Wen X (2019). Chitosan functionalized activated coke for Au nanoparticles anchoring Green synthesis and catalytic activities in hydrogenation of nitrophenols and azo dyes. Applied Catalysis B: Environmental 255:117740.

Gadipelly C, Mannepalli LK (2019) Nano-metal oxides for organic transformations. Current opinion in Green and Sustainable Chemistry 15:20-26

Geng X, Luo Y, Zheng B, Zhang C (2017). Photon assisted room-temperature hydrogen sensors using PdO loaded WO_3 nanohybrids. International Journal of Hydrogen Energy 42(9):6425-6434.

Hassan ME, Chen Y, Liu G, Zhu D, Cai J (2016). Heterogeneous photo-Fenton degradation of methyl orange by Fe_2O_3/TiO_2 nanoparticles under visible light. Journal of Water Process Engineering 12:52-57.

Kang M, Liang J, Wang F, Chen X, Lu Y, Zhang J (2020). Structural design of hexagonal/monoclinic WO_3 phase junction for photo catalytic degradation. Materials Research Bulletin 121:110614.

Katheresan V, Kansedo J, Lau SY (2018). Efficiency of various recent wastewater dye removal methods: A review. Journal of Environmental Chemical Engineering 6(4):4676-4697.

Kolhe PS, Mutadak P, Maiti N, Sonawane KM (2020). Synthesis of WO_3 Nanoflakes by Hydrothermal Route and its Gas Sensing Application, Sensors and Actuators. A. Physical 304:111877.

Li M, Sun M, Dong H, Zhang J, Su Y, Qiang Z (2020). Enhancement of micropollutant degradation in UV/H_2O_2 process via iron-containing coagulants. Water Research 172:115497.

Liu S, Zeng W, Li Y (2019). Synthesis of spherical WO_3-H_2O network for ethanol sensing application. Materials letters 253:42-45.

Liu Y, Liu X, Zhao Y, Dionysiou DD (2017). Aligned α-FeOOH nanorods anchored on a grapheme oxide-carbon nanotubes aerogel can serve as an effective Fenton-like oxidation catalyst. Applied Catalysis B: Environmental 213:74-86.

Lousada CM, Brinck T, Jonsson M (2015). Application of reactivity descriptors to the catalytic decomposition of hydrogen peroxide at oxide surfaces. Computational and Theoretical Chemistry 1070:108-116.

Omri A, Hamza W, Benzina M (2020) Photo-Fenton oxidation and mineralization of methyl orange using Fe-sand as effective heterogeneous catalyst. Journal of Photochemistry and Photobiology A: Chemistry 393:112444.

Osgouei MS, Khatamian M, Kakili H (2020). Improved visible-light photocatalytic activity of Mn_3O_4-based nanocomposites in removal of methyl orange. Materials Chemistry and Physics 239:122108.

Parthibavarman M, Karthik M, Prabhakaran S (2018). Facile and one step synthesis of WO_3 nanorods and nanosheets as an efficient photocatalyst and humidity sensing material. Vacuum 155:224-232.

Pavithra GK, Senthil KP, Jaikumar V, Rajan SP (2019). Removal of colorants from wastewater: A review on sources and treatment strategies. Journal of Industrial and Engineering Chemistry 75:1-19.

Perfecto TM, Zito CA, Volanti DP (2016). Room-temperature volatile organic compounds sensing based on WO_3·0.33H_2O, hexagonal-WO_3, and their reduced graphene oxide composites. Royal Society of Chemistry Advances 6(107):105171-105179.

Rajasulochana P, Preethy V (2016). Comparison on efficiency of various techniques in treatment of waste and sewage water-A comprehensive review. Resource-Efficient Technologies 2(4):175-184.

Salkar AV, Naik AP, Joshi VS, Haram SK, Morajkar PP (2018). Designing a 3D nanoporous network: Via self-assembly of WO_3 nanorods for improved electrocapacitive performance. CrystEngComm 20(42):6683-6694.

Seo C, Shin J, Lee M, Lee W, Yoom H, Son H, Jang S, Lee Y (2019). Elimination efficiency of organic UV filters during ozonation and UV/H_2O_2 treatment of drinking water and wastewater effluent. Chemosphere 230:248-257.

Thornburg NE, Nauert SL, Thompson AB, Notestein JM (2016). Synthesis-Structure-Function Relationships of Silica-Supported Niobium (V) Catalysts for Alkene Epoxidation with H_2O_2. ACS Catalysis 6(9):6124-6134.

Wang N, Zheng T, Zhang G, Wang P (2016). A review on Fenton-like processes for organic wastewater treatment. Journal of Environmental Chemical Engineering 4(1):762-787.

Wardenier N, Liu Z, Nikiforov A, Van Hulle SWH, Leys C (2019). Micropollutant elimination by O_3, UV and plasma-based AOPs: An evaluation of treatment and energy costs. Chemosphere 234:715-724.

Wei X, Wang Y, Feng Y, Xie X, Li X, Yang S (2019). Different adsorption-degradation behavior of methylene blue and Congo red in nanoceria/H_2O_2 system under alkaline conditions. Scientific reports 9(1):4964.

Wiedmer D, Sagstuen E, Welch K, Haugen HJ, Tiainen H (2016). Oxidative power of aqueous non-irradiated TiO_2-H_2O_2 suspensions: Methylene blue degradation and the role of reactive oxygen species. Applied Catalysis B: Environmental 198:9-15.

Wolski L, Walkowiak A, Ziolek M (2019). Formation of reactive oxygen species upon interaction of Au/ZnO with H_2O_2 and their activity in methylene blue degradation. Catalysis Today 333:54-62.

Xiao J, Wang C, Liu H (2020), Fenton-like degradation of dimethyl phthalate enhanced by quinone species. Journal of Hazardous Materials 382:121007.

Yang J, Liang Y, Li K, Yang G, Yin S (2019). One-step low-temperature synthesis of 0D CeO_2 quantum dots/2D BiOX (X= Cl, Br) nanoplates heterojunctions fir highly boosting photo-oxidation and reduction ability. Applied Catalysis B: Environmental 250:17-30.

Yang J, Liang Y, Li K, Yang G, Zhu Y, Liu S, Lei W (2018). New Reaction pathway induced by the synergistic effects of Bi Plasmon and La^{3+} doping fir efficient visible light photocatalytic reaction on BioCl. Applied surface science 458:769-780.

Zeng L, Zhe F, Wang Y, Zhang Q, Ge S, Zhao Y, Lin H (2019). Preparation of interstitial carbon doped BiOI for enhanced performance in photocatalytic nitrogen fixation and methyl orange degradation. Journal of Colloid and Interface Science 539:563-574.

Zhang F, Dong G, Wang M, Zeng Y, Wang C (2018). Efficient removal of methyl orange using Cu_2O as dual function catalyst. Applied Surface Science 444:559-568.

Zhang MH, Dong Hu, Zhao L, Wang DX, Meng Di (2019). A review on Fenton process for organic wastewater treatment based on

optimization perspective. Science of the Total Environment 670:110-121.
Zhu Y, Zhu R, Xi Y, Zhu J (2019). Strategies for enhancing the heterogeneous Fenton catalytic reactivity: A review; Applied Catalysis B: Environmental 255:117739.
Ziolek M, Sobczak I (2017). The role of niobium component in heterogeneous catalysts. Catalysis Today 285:211-225.
Ziolek M, Sobczak I, Decyk P, Sobańska K, Pietrzyk P, Sojka Z (2015). Search for reactive intermediates in catalytic oxidation with hydrogen peroxide over amorphous niobium (V) and tantalum (V) oxides. Applied Catalysis B: Environmental 164:288-296.